



OPEN

Expression and processing of mature human frataxin after gene therapy in mice

Teerapat Rojsajakul¹, Nithya Selvan², Bishnu De³, Jonathan B. Rosenberg³, Stephen M. Kaminsky³, Dolan Sondhi³, Peter Janki², Ronald G. Crystal³, Clementina Mesaros¹, Richie Khanna² & Ian A. Blair^{1✉}

Friedreich's ataxia is a degenerative and progressive multisystem disorder caused by mutations in the highly conserved frataxin (FXN) gene that results in FXN protein deficiency and mitochondrial dysfunction. While gene therapy approaches are promising, consistent induction of therapeutic FXN protein expression that is sub-toxic has proven challenging, and numerous therapeutic approaches are being tested in animal models. FXN (hFXN in humans, mFXN in mice) is proteolytically modified in mitochondria to produce mature FXN. However, unlike endogenous hFXN, endogenous mFXN is further processed into N-terminally truncated, extra-mitochondrial mFXN forms of unknown function. This study assessed mature exogenous hFXN expression levels in the heart and liver of C57Bl/6 mice 7–10 months after intravenous administration of a recombinant adeno-associated virus encoding hFXN (AAVrh.10hFXN) and examined the potential for hFXN truncation in mice. AAVrh.10hFXN induced dose-dependent expression of hFXN in the heart and liver. Interestingly, hFXN was processed into truncated forms, but found at lower levels than mature hFXN. However, the truncations were at different positions than mFXN. AAVrh.10hFXN induced mature hFXN expression in mouse heart and liver at levels that approximated endogenous mFXN levels. These results suggest that AAVrh.10hFXN can likely induce expression of therapeutic levels of mature hFXN in mice.

Friedreich's ataxia (FRDA) is the most common inherited ataxia, affecting approximately 1 in 50,000 of the Caucasian population in the US¹. Symptoms include dysarthria (slurred speech), spasticity, scoliosis, diabetes, progressive ataxia, and cardiomyopathy^{1–6}. Prognosis is poor, with patients slowly progressing to wheelchair dependency (usually in their late teens or early twenties²) and the majority dying from heart disease between the ages of 16 and 41^{7,8}. While there are currently no curative treatments for the cardiac manifestations of FRDA, numerous therapeutic approaches are being tested in pre-clinical models^{9–11}. As FRDA is a genetic disease caused by an autosomal recessive mutation in the frataxin gene (*FXN*) that encodes the highly conserved frataxin protein (FXN), genetic approaches for treatment are under investigation^{12–14}. FRDA-related mutations classically consist of a trinucleotide (GAA) repeat expansion within the first *FXN* intron, which results in DNA triplex formation, epigenetic silencing, and consequently reduced FXN protein production^{15–17}. While the intracellular role of FXN has not been clearly defined^{18,19}, FXN deficiency compromises iron-sulfur (Fe-S) cluster biosynthesis, leading to mitochondrial iron overload, mitochondrial dysfunction, and oxidative stress²⁰ that can culminate in the neuro- and cardio-degeneration characteristics of FRDA^{21–24}.

Gene replacement (e.g., gene therapy) represents a promising approach to treating FRDA^{10,11}. One of the pivotal challenges critical to the success of gene therapy is to induce sufficient FXN protein expression to achieve therapeutic efficacy while limiting the toxicity induced by its overexpression, which can result in impaired Fe-S biogenesis and cellular/mitochondrial function, and eventually lead to cell death¹⁷. Previous gene therapy studies conducted in mouse models have shown mature hFXN expression at levels that cause cardiotoxicity and hepatotoxicity, leading to reduced efficacy^{25,26}. Thus, gene replacement approaches for FRDA continue to require detailed study in animal models to optimize efficacy and minimize toxicity in human studies.

While FXN is highly conserved, species-specific processing results in diverse populations of mature FXN variants. Full-length hFXN (1–210) is expressed in the cytosol of nucleated cells and translocates to mitochondria

¹Department of Systems Pharmacology and Translational Therapeutics Perelman School of Medicine, Penn/CHOP Friedreich's Ataxia Center of Excellence, Center of Excellence in Environmental Toxicology, University of Pennsylvania, Philadelphia, PA, USA. ²LEXEO Therapeutics, Inc, New York, NY, USA. ³Department of Genetic Medicine, Weill Cornell College of Medicine, New York, NY, USA. ✉email: ianblair@upenn.edu

for two-step removal of the mitochondrial targeting sequence by mitochondrial processing peptidase (MPP)²⁷. This results in production of a 130-amino acid, mitochondrial mature hFXN protein (81–210, Fig. 1)^{28,29}. In addition to this hFXN form, an alternatively spliced, N-terminally acetylated (methionine-76) extra-mitochondrial, 135-amino acid hFXN form was discovered in human erythrocytes and termed hFXN-E^{24,30}. Mitochondrial mature hFXN and extra-mitochondrial mature hFXN-E proteins are not secreted into systemic circulation but can be quantified in whole blood of healthy control subjects and FRDA patients^{16,17}. A high-resolution mass spectrometry (HRMS)-based method was developed for the analysis of hFXN to characterize mitochondrial mature mouse FXN (mFXN, 78–207; Fig. 1), which is thought to arise by the same MPP-dependent mechanism as mature hFXN^{31,32}. However, it was found that mice also form a major extra-mitochondrial form of mature mFXN in which the N-terminal leucine residue is lost to generate a cytosolic 129-amino acid truncated protein with an N-terminal tryptic peptide at the amino terminus (G⁷⁹TLDNPSSLDETAYER⁹⁴; Fig. 1)³¹. Other mFXN truncations include a major N-3 truncation that gives rise to a mature mFXN proteoform in the liver with an N-terminal L⁸¹DNPSSLDETAYER⁹⁴ peptide (Fig. 1)³¹. Interestingly, hFXN does not undergo such processing to form truncated extra-mitochondrial forms in humans^{28,29}, and mice cannot produce the alternatively spliced extra-mitochondrial FXN form observed in humans and non-human primates as mFXN lacks the corresponding methionine-76 residue of hFXN³¹. Thus, while mitochondrial mature hFXN and mFXN arise by similar mechanisms, species-specific variants exist and must be considered in pre-clinical studies on hFXN gene therapy.

The primary objective of this pre-clinical study was to determine whether intravenous (IV) gene therapy with recombinant adeno-associated virus rhesus serotype 10 encoding hFXN (AAVrh.10hFXN) could drive expression of mature hFXN in wild-type (WT) mice at levels that approximate endogenous mature mFXN³¹ using a two-dimensional nano-ultra-high performance liquid chromatography-parallel reaction monitoring (2D-nano-UHPLC-PRM/HRMS) method³¹ to quantify both endogenous mature mFXN and exogenous mature hFXN in heart and liver tissues. The secondary objective of this study was to determine whether hFXN expressed in mouse tissues undergoes truncation—a process that does not occur in human tissues³¹.

Methods

Reagents and supplies

All reagents and solvents were liquid chromatography (LC)/mass spectrometry (MS)-grade quality unless otherwise noted. [¹³C₆]-leucine was obtained from Cambridge Isotope Laboratories (Andover, MA). Anti-FXN recombinant rabbit monoclonal antibody (mAb) EPR21840 (cat. # ab219414) was from Abcam (Cambridge, UK). Ethylenediaminetetraacetic acid (EDTA)-free protease inhibitor cocktail, DL-dithiothreitol (DTT), EDTA-free Easypack protease inhibitor cocktail tablets, and dimethyl pimelimidate dihydrochloride (DMP) were purchased from MilliporeSigma (Billerica, MA). LC-grade water and acetonitrile were obtained from Burdick and Jackson (Muskegon, MI). Protein G Dynabeads for immunoprecipitation (IP) and radioimmunoprecipitation assay (RIPA) lysis buffer with EDTA were from ThermoFisher Scientific (Waltham, MA). LC/MS grade water and Optima LC/MS grade solvents were from Fisher Scientific (Pittsburgh, PA).

		10	20	30	40	MPP	50
Q16595 HUMAN		MWTLGRRAVA	GLLASPSPAQ	AQTLTRVPRP	AELAPLCGRR	↓	GLRTDIDATC
Q35943 MOUSE		MWAFGGRAAV	GLLPRTAS-R	ASAWVGNPRW	REPIVTCGRR		GLHVTVNAGA
		60	70	80	MPP	90	100
Q16595 HUMAN		TPRRASSNQR	GLNQIWNVKK	QSVYLMNLRK	↓	SGTLGHGPGSL	DETTYERLAE
Q35943 MOUSE		TRH--AHLNL	HYLQILNIKK	QSVCVVHLRN		LGTLDNPSSL	DETAYERLAE
		110	120	130	140	150	
Q16595 HUMAN		ETLDSLAEFF	EDLADKPYTF	EDYDVSFGSG	VLTVKLGDDL	GTIVINKQTP	
Q35943 MOUSE		ETLDSLAEFF	EDLADKPYTL	EDYDVSFGDG	VLTIKLGDDL	GTIVINKQTP	
		160	170	180	190	200	
Q16595 HUMAN		NKQIWLSSPS	SGPKRYDWTG	KNWVYSHDGV	SLHELLAAEL	TKALKTKLDL	
Q35943 MOUSE		NKQIWLSSPS	SGPKRYDWTG	KNWVYSHDGV	SLHELLAREL	TKALNTKLDL	
		210					
Q16595 HUMAN		SSLAYSGKDA					
Q35943 MOUSE		SSLAYSGKGT					

— Human mitochondrial mature frataxin tryptic peptide
— Mouse mitochondrial mature frataxin tryptic peptide
- - - - - Mouse cytosolic mature frataxin tryptic peptide

Figure 1. Alignment of mature hFXN (Uniprot Q16595) and mFXN (Uniprot Q35943). Amino acids in green are specific to hFXN while those in purple are specific to mFXN. Translocation of full-length FXN to the mitochondria followed by two sequential cleavages by MPP results in the formation of mature hFXN and mFXN as 130 amino acid proteins. Quantification of mature hFXN is based on the S⁸¹GTLGHGPGSLDETAYER⁹⁷ tryptic peptide (N), while quantification of mature mFXN is based on the L⁷⁸GTLDNPSSLDETAYER⁹⁴ tryptic peptide (N). Extra-mitochondrial mature mFXN is formed through an unknown mechanism and is detected as the truncated N-1 tryptic peptide G⁷⁹TLDNPSSLDETAYER⁹⁴. Other proteoforms are detected by further truncations on the N-terminal tryptic peptide as N-2, N-3, N-4, N-5, and N-6. hFXN = human frataxin; mFXN = mouse frataxin; MPP = mitochondrial processing peptidase.

Study animals

The study was conducted in accordance with ARRIVE guidelines described more comprehensively by Percie du Sert et al.³³. C57Bl/6 mice were received from Taconic Biosciences (Germantown, NY) and were weighed and identified by ear punch upon receipt. Animals were housed by sex and treatment group in normal vivarium cages, with up to four mice per cage. Temperature and relative humidity were maintained at 21–23 °C and 45–55%, respectively, and were monitored by Watchdog Environmental Monitors (VERTIV; Lincoln, NE). Animals were exposed to a 12:12 h light:dark cycle that alternated at 6 am and 6 pm. Water was supplied through an automated watering system, and the water pH was maintained at 2.5–2.8 (monitored weekly). Food was provided ad libitum (PicoLab® Rodent Diet 20; cat. # 5053; Lab Supply; Northlake, TX).

Dosing and sampling

For the purposes of 2D-nano-UHPLC-PRM/HRMS analysis, eight-week-old (± 1 week) WT C57Bl/6 mice weighing between 18 and 30 g were IV-administered vehicle [control article/formulation buffer (phosphate-buffered saline [PBS], pH 7.4; 1.06 mM KH_2PO_4 , 155.17 mL NaCl, 2.97 mM $\text{Na}_2\text{PO}_4 \cdot 7\text{H}_2\text{O}$)] or a low [1.8×10^{12} genome copies (gc)/kg], mid (5.7×10^{12} gc/kg), or high (1.8×10^{13} gc/kg) dose of AAVrh.10hFXN. Vector titration was performed by quantitative polymerase chain reaction (data not shown). Administration was performed in a volume of 0.1 mL by IV injection into the lateral veins of the tail. The control group ($n = 5$) comprised three males and two females, the low-dose group ($n = 6$) comprised three males and three females, the mid-dose group ($n = 6$) comprised three males and three females, and the high-dose group ($n = 8$) comprised three males and five females. Animals were excluded from the study when the IV injection leaked subcutaneously or externally, mice did not survive for 48-h post injection, or dermatitis and/or any signs of severe stress and pain were noted 48 h after injection. Mice were anesthetized by CO_2 inhalation until surgical plane, then euthanized by terminal cardiocentesis 7–10 months after dosing. Heart (septum) and liver were collected, weighed, and snap-frozen on dry ice and stored at -80 °C (± 10 °C) until further processing.

Internal standard

It was possible to determine whether truncation of the FXN proteins had occurred in vivo in the mice or during sample processing by adding an internal standard (stable isotope labelling by amino acids in cell culture [SILAC]-hFXN [$[\text{S}^{81}\text{GTLGHPGSLDETTYER}^{97}]$] in which the $[\text{C}_6^{12}]$ -lysine and $[\text{C}_6^{12}]$ -leucine were replaced with $[\text{C}_6^{13}\text{N}_6^{15}]$ -lysine and $[\text{C}_6^{13}]$ -leucine), to tissue samples before the analysis (Fig. 2). Mature SILAC-hFXN (81–210) is 98.5% homologous and 92.3% identical to the predicted sequence of mature mFXN (78–207). The hFXN

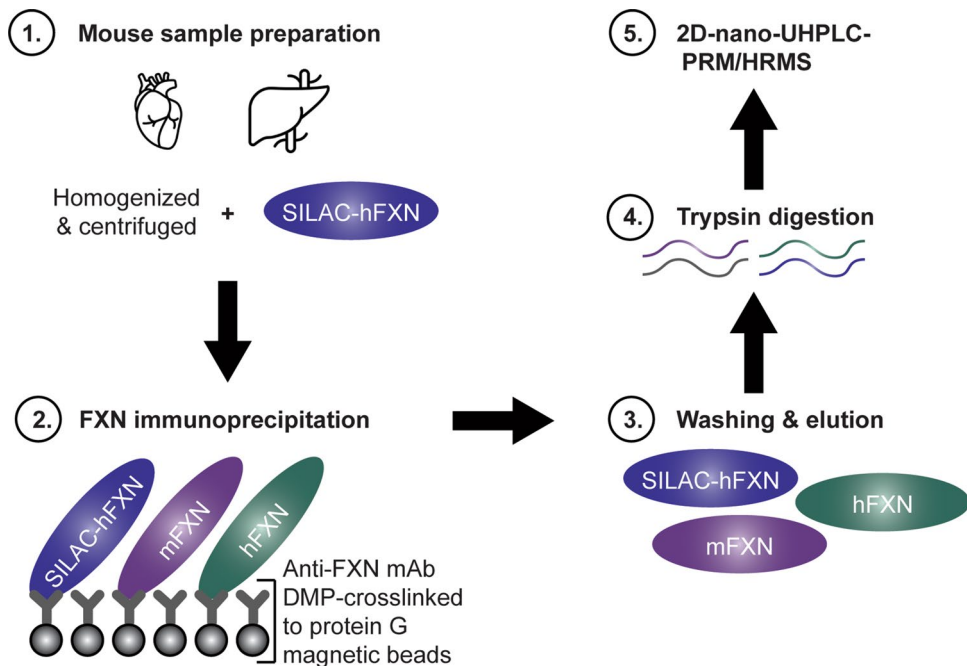


Figure 2. Workflow for quantification of mature hFXN and mFXN. Covalent linking of a rabbit mAb to protein G beads facilitated efficient recovery of mFXN and hFXN proteoforms from tissues for 2D-nano-UHPLC-PRM/HRMS analysis, as it allowed the beads to be washed to remove matrix contaminants. 2D-nano-UHPLC-PRM/HRMS = two-dimensional nano-ultra-high performance liquid chromatography-parallel reaction monitoring high-resolution mass spectrometry; DMP = dimethyl pimelimidate dihydrochloride; FXN = frataxin; hFXN = human frataxin; mAb = monoclonal antibody; mFXN = mouse frataxin; SILAC = stable isotope labelling by amino acids in cell culture.

protein standard was prepared with a 6× His tag and the SILAC-hFXN internal standard prepared with a 6× His tag as previously described^{30,32}.

Tissue lysis

Mouse heart and liver tissue samples were cut into small pieces while still frozen, and 7–100 mg pieces were transferred to LoBind Eppendorf tubes containing 1 mL RIPA lysis buffer (supplemented with 1 mM EDTA, 1× complete protease cocktail, 1 mM DTT). Tissue homogenization was conducted on ice using a sonication probe (30 pulses at setting 5). Lysed samples were centrifuged at 17,000×g at 4 °C for 10 min and the supernatant transferred to a separate tube. For heart samples, 50 ng of SILAC-hFXN standard was added and the entire sample was analyzed. For liver samples, 500 µL of the homogenate (~50%) was withdrawn, and 50 ng of SILAC-hFXN standard was added (i.e., only half of the sample was analyzed). Sample volumes were adjusted to standardize tissue amounts across samples.

mAb-bead cross-linking

Anti-FXN recombinant rabbit mAb (Abcam; Cambridge, UK; cat. # ab21914) was cross-linked to magnetic protein G beads using DMP³⁰ without any loss of mature mFXN or hFXN immunoreactivity (Fig. 2). This made it possible to thoroughly wash the beads to remove all interfering matrix contaminants before eluting the mature FXN proteoforms for 2D-nano-UHPLC-PRM/HRMS analysis, unlike previous IP studies³¹. Analyses could then be conducted without contamination of the mass spectrometer's ion source or degradation of the LC column. Protein G magnetic Dynabeads (5 mg; 165 µL; ThermoFisher Scientific; Waltham, MA; cat. # 10009D) were washed three times with PBS containing 0.02% Tween (buffer A) and incubated with 40 µg (40 µL in 460 µL PBS) of a recombinant rabbit mAb against the FXN protein (cross-reactive with both mFXN and hFXN) on a rotator at 4 °C overnight. The mAb-bound protein G beads were washed twice with 1 mL cross-linking buffer (0.2 M triethanolamine, pH 8.0) and incubated with 13 mg DMP in 2 mL cross-linking buffer on a rotator at room temperature for 1 h. The mAb-crosslinked G beads were quenched with 2 mL blocking solution (0.1 ethanolamine, pH 8.5) for 1 h at room temperature. The beads were washed with buffer A three times and stored in 1 mL of buffer A at 4 °C until used (Fig. 2).

FXN IP

FXN protein IP was performed following a previously described protocol with minor modifications³¹. Briefly, a portion of tissue homogenate (typically 500 µL) was mixed with 500 µL ice-cold RIPA lysis buffer (supplemented with 1× complete protease cocktail, 1 mM DTT). Mature SILAC-hFXN (50 ng) containing [¹³C₆]-Leucine was spiked into each sample to serve as the internal standard. Each sample was transferred to a 2 mL LoBind Eppendorf tube containing 100 µL G beads cross-linked to an FXN mAb (0.5 mg) and incubated on a rotator at 4 °C overnight. The next day, the supernatant was removed, and the cross-linked beads were washed two times with 1 mL buffer A. The beads were then transferred to a LoBind Eppendorf tube and washed with 1 mL PBS. Next, 100 µL elution buffer (300 mM acetic acid and 10% acetonitrile) was added to the beads, which were eluted at 1,000 rpm at 37 °C for 1 h. The elution buffer was then transferred to another 1.5 mL LoBind Eppendorf and dried under nitrogen flow. Dried samples were then dissolved in 50 µL 25 mM aqueous NH₄HCO₃ solution containing 500 ng trypsin protease and digestion was performed at 37 °C overnight prior to 2D-nano-UHPLC-PRM/HRMS analysis. Calibration standards were prepared by spiking 1, 2, 15, 30, 50, 600 and 1500 ng of mature hFXN into a solution of 50 ng of mature SILAC-hFXN in 5% bovine serum albumin (BSA), and analysis of the calibration standards was performed alongside the samples following the same protocol.

Standard curves

Linear standard curves were obtained for the FXN peptide S⁸¹GTLGHPGSLDETTYER⁹⁷) used to calculate mFXN and hFXN levels over a 1–50 ng range as previously described³⁴ (a representative standard curve shown in Supplementary Fig. S1a). Different standard curves were used to quantify mFXN and hFXN > 50 ng, as these quantities distorted the lower end of the curve (Supplementary Fig. S1b). Transitions that were used to monitor the peptides are shown in Supplementary Table S1. Back-calculated values for the authentic standards used to prepare the standard curves were within acceptable limits (Supplementary Table S2).

2D-nano-UHPLC-PRM/HRMS

Analyses were conducted using a high-resolution Q-Exactive HF hybrid quadrupole-orbitrap mass spectrometer coupled to a Dionex Ultimate 3000 RSLCnano with capillary flowmeter chromatographic systems (ThermoFisher Scientific; San Jose, CA) as previously described with minor modifications (Fig. 2)³¹. The 2D system was set up in a pre-concentration mode composed of a ten-port valve, one nanopump for delivering solvents to analytical columns, and a micropump for delivering solvents to trapping columns. The 2D-nano-UHPLC-PRM/HRMS system was controlled by Xcalibur software (version 4.3) from the Q-Exactive mass spectrometer. The UHPLC trapping column was an Acclaim PepMap C18 cartridge (0.3 mm × 5 mm, 100 Å; ThermoFisher Scientific; San Jose, CA) and the analytical column was a C18 AQ nano-UHPLC column with a 10 µm pulled tip (75 µm × 25 cm, 3 µm particle size; Columntip; New Haven, CT). Samples (8 µL) were injected using the microliter-pickup injection mode. Loading solvent was water:acetonitrile (99.7:0.3 v:v) containing 0.2% formic acid. During sample loading, the valve stayed in the loading position (1–2) and solvent was loaded at 10 µL/min for 3 min. During the elution and analysis steps, the valve stayed in the injection position (1–10), the trapping column was connected to the nanopump and the analytical column, and samples were back-flushed into the analytical column. Washing of the trapping column using the nanopump continued until 5 min before the end of the run. Samples were eluted in the mass spectrometer with a linear gradient at a flow rate of 0.4 µL/min. Solvent A was water:acetonitrile

(99.5:0.5 v:v) containing 0.1% formic acid, and solvent B was acetonitrile:water (98:2 v:v) containing 0.1% formic acid. The gradient on the analytical column was as follows: 2% B at the start, 5% B at 10 min, 55% B at 45 min, 98% B at 60 min, held for 15 min, then re-equilibrated at 2% B from 70 to 80 min. Ionization was conducted using a Nanospray Flex ion source (ThermoFisher Scientific; San Jose, CA). Mass spectrometer operating conditions were as follows: spray voltage = 3500 V; ion transfer capillary temperature = 275 °C; ion polarity = positive; S-lens radiofrequency (RF) level = 55; and in-source collision-induced dissociation (CID) = 1.0 eV. The PRM/HRMS parameters were as follows: resolution = 60,000; automatic gain control (AGC) target = 2e5; maximum ion trap (IT) = 80 ms; loop count = 5; isolation window = 2.0 Da; and normalized collision energy (NCE) = 25 (Supplementary Table S1).

Data analyses

Protein quantification was performed using Skyline software (version 23.1; MacCoss Laboratory, University of Washington; Seattle, WA)³⁵. The peak area ratio of each PRM/HRMS transition for each unlabeled/light (L) peptide to labeled/heavy (H) peptide was calculated by Skyline software and used for absolute quantification. The most intense PRM/HRMS transition of $[M + 3H]^{3+}$ (m/z 611.3002) to y^{4+} (568.2726) transition for $S^{81}GTLGHPGSLDETTYER^{97}$ (L = [$^{13}C_6$]-leucine) was used for the internal standard. The most intense PRM/HRMS transition of $[M + 2H]^{2+}$ (m/z 940.9473) to y^{7+} (m/z 883.3792) for $L^{78}GTLDNPSSLDETAYER^{94}$ was used to quantify mature mFXN. The most intense PRM/HRMS transition of $[M + 3H]^{3+}$ (m/z 607.2867) to y^{4+} (m/z 568.2726) for $S^{81}GTLGHPGSLDETTYER^{97}$ was used to quantify mature hFXN. Concentrations of mature mFXN and hFXN were determined from the L/H ratio of each N-terminal peptide to $S^{81}GTLGHPGSLDETTYER^{97}$ and interpolation from the standard curve.

Ethics declarations

All animal protocols and surgical experiments on mice were performed in accordance with and approved by the Institutional Animal Care and Use Committee (IACUC) of the Belfer Gene Therapy Core Facility/Weill Cornell Medicine.

Results

Effect of hFXN gene therapy on mature mFXN levels in mouse heart tissue

2D-nano-UHPLC-PRM/HRMS was used to detect mature mFXN and its truncated forms in the mouse heart following hFXN gene therapy. A representative chromatogram of mature mFXN in the mouse heart is shown in Fig. 3a. There was robust detection of the N-terminal peptide (SGTLGHPGSLDETTYER) of the mature form of the internal standard (SILAC-hFXN), the mature mFXN N-terminal peptide (LGTDNPSSLDETAYER [denoted N]), and the N-terminally truncated mFXN proteoforms (denoted N minus 1 to N minus 6 [N-1 to N-6]). Further, the analysis revealed a lack of proteolysis during the analytical procedure, as only product ions from MH_3^{3+} from the internal standard N-terminal tryptic-peptide $S^{81}GTLGHPGSLDETTYER^{97}$ were detected (Fig. 3a). In contrast, product ions from MH_2^{2+} (including the intense y_7^{+} -ion) of the predicted (N-1)-mFXN tryptic-peptide $G^{79}TLDNPSSLDETAYER^{94}$ were present in mouse heart, together with relatively weak product ions derived from three other major truncated forms (N-2, N-3, and N-6; Fig. 3a). These findings are very similar to those reported for mice that did not undergo gene therapy, indicating that gene therapy did not alter endogenous mFXN biosynthesis in the heart³¹.

Levels of mature mFXN were next measured in the mouse heart following administration of vehicle or low-dose (1.8e12 gc/kg), mid-dose (5.7e12 gc/kg), or high-dose (1.8e13 gc/kg) AAVrh.10hFXN. 2D-nano-UHPLC-PRM/HRMS ion transitions used for the analysis of mature FXN forms are shown in Supplementary Table S1. Mean levels of total mature mFXN in heart tissue of mice receiving one of three AAVrh.10hFXN doses ranged from a low of 1.3 to a high of 193.5 ng/mg tissue with an average of 25.6 ± 9.0 ng/mg (mean ± s.e.m.; n = 23; median = 7.7 ng/mg) and showed no dose-dependence (Fig. 3b and Supplementary Table S3). The relative abundance of the N peptide (compared with truncated mFXN forms) remained remarkably constant in the heart (14.5%; Fig. 3c and Supplementary Table S3), with levels approximating those reported in mice not subjected to gene therapy in a previous study³¹. The N-1 proteoform was the most abundant and represented 67.6% of total mature mFXN (Fig. 3c and Supplementary Table S3). The mFXN tryptic peptide $N^{77}LGTDNPSSLDETAYER^{97}$, denoted N + 1, was monitored to determine whether full length mFXN or elongated forms (compared to mature mFXN) resulting from alternate splicing³⁶ or inhibition of MPP^{28,29} were present in mouse hearts. The N + 1 peptide represented an overall mean of only 0.1% of total mFXN in the mouse heart (n = 23) (Fig. 3a and Supplementary Table S3). This indicated near-complete processing of full length/elongated mFXN or alternately spliced mFXN, if present, into mature/truncated mFXN proteoforms.

Effect of hFXN gene therapy on mature mFXN levels in mouse liver tissue

A representative 2D-nano-UHPLS-PRM/HRMS chromatogram of mature mFXN in the mouse liver is shown in Fig. 4a. Similar to heart tissue findings, in mouse liver there was robust detection of the mature SILAC-hFXN internal standard N-terminal peptide (SGTLGHPGSLDETTYER), the mFXN N peptide (LGTDNPSSLDETAYER), and the N-terminally truncated forms (N-1 to N-6). These results indicate that synthesis and processing of endogenous mFXN in the liver is not altered following AAVrh.10hFXN gene therapy, as similar findings were observed in mice that did not undergo gene therapy³¹. Levels of mature mFXN were measured in the mouse liver following administration of vehicle or low-dose (1.8e12 gc/kg), mid-dose (5.7e12 gc/kg), or high-dose (1.8e13 gc/kg) AAVrh.10hFXN. Mean levels of total mature mFXN in mouse liver administered vehicle or one of the three AAVrh.10hFXN doses ranged from a low of 2.7 to a high of 81.7 ng/mg tissue, or an average of 14.9 ± 3.9 ng/mg (mean ± s.e.m.; n = 25; median = 9.5 ng/mg) and showed no dose-dependence (Fig. 4b and Supplementary

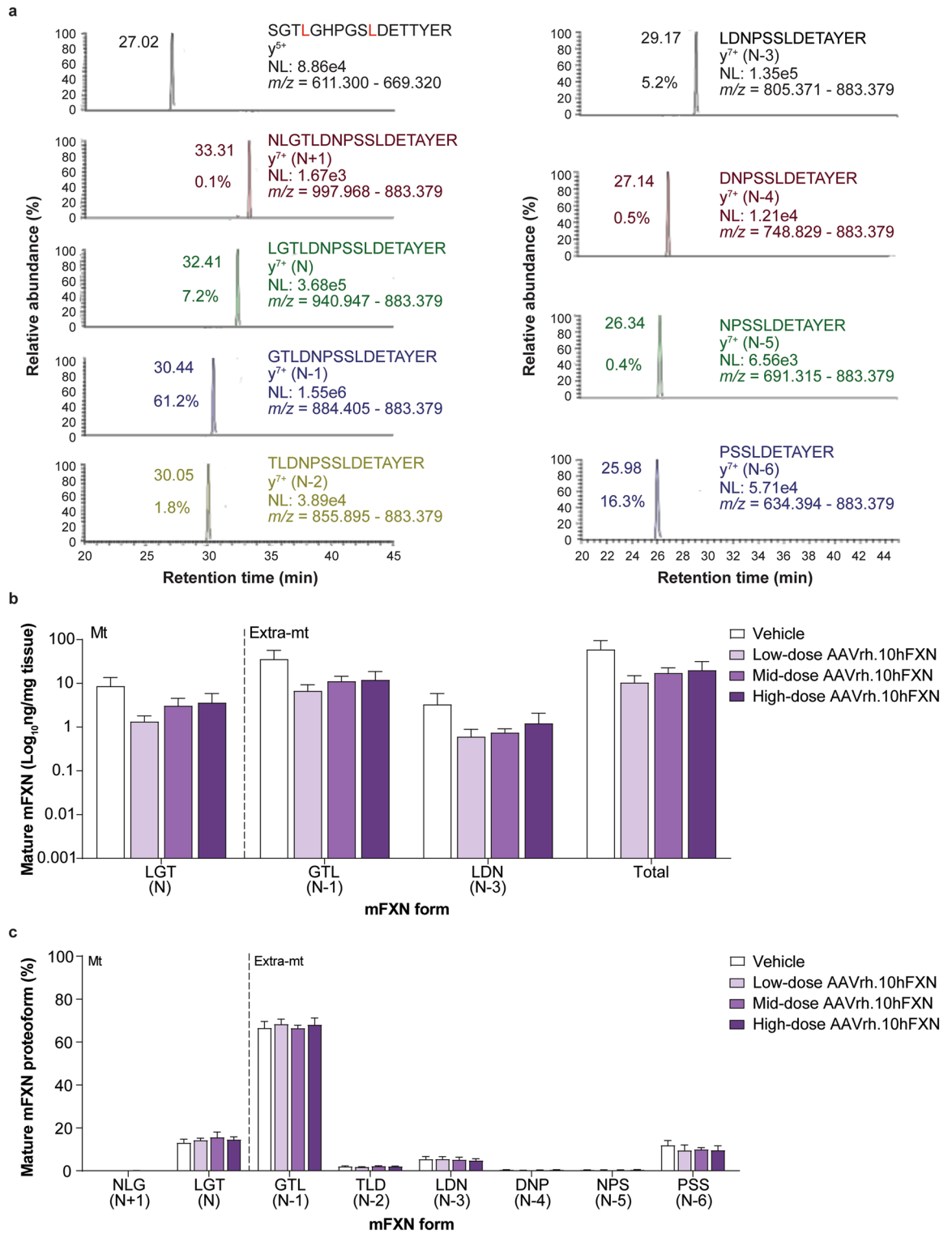


Figure 3. Detection and quantification of mature mFXN and its N-terminal tryptic peptides in the mouse heart following hFXN gene therapy. **(a)** Representative chromatograms from 2D-nano-UHPLC-PRM/HRMS analysis of mature mFXN N-terminal tryptic peptides in the heart of a mouse administered a high dose (1.8e13 gc/kg) of AAVrh.10hFXN. y-ion indicates the number of amino acids from the carboxy terminus that are present in this ion. Peptide retention times and relative amounts are shown on the left of the relevant signal. **(b)** Absolute concentrations of Mt and Extra-mt mature mFXN proteoforms in mouse heart after administration of one of three different doses of AAVrh.10hFXN (low dose = 1.8e12 gc/kg, n = 6; mid dose = 5.7e12 gc/kg, n = 4; high dose = 1.8e13 gc/kg, n = 8) or vehicle (n = 5). While there were six mice treated with mid-dose AAVrh.10hFXN, insufficient heart sample precluded analysis of two mice. **(c)** Relative amounts of mature mFXN proteoforms in mice after administration of the same doses of AAVrh.10hFXN or vehicle (sample sizes as above). **(b, c)** Data are expressed as mean ± s.e.m. 2D-nano-UHPLC-PRM/HRMS = two-dimensional nano-ultra-high performance liquid chromatography-parallel reaction monitoring high-resolution mass spectrometry; AAVrh.10hFXN = adeno-associated virus rhesus serotype 10 encoding human frataxin; Extra-mt = extra-mitochondrial; hFXN = human frataxin; mFXN = mouse frataxin; Mt = mitochondrial; m/z = mass-to-charge ratio; NL = normalized signal level; s.e.m. = standard error of the mean.

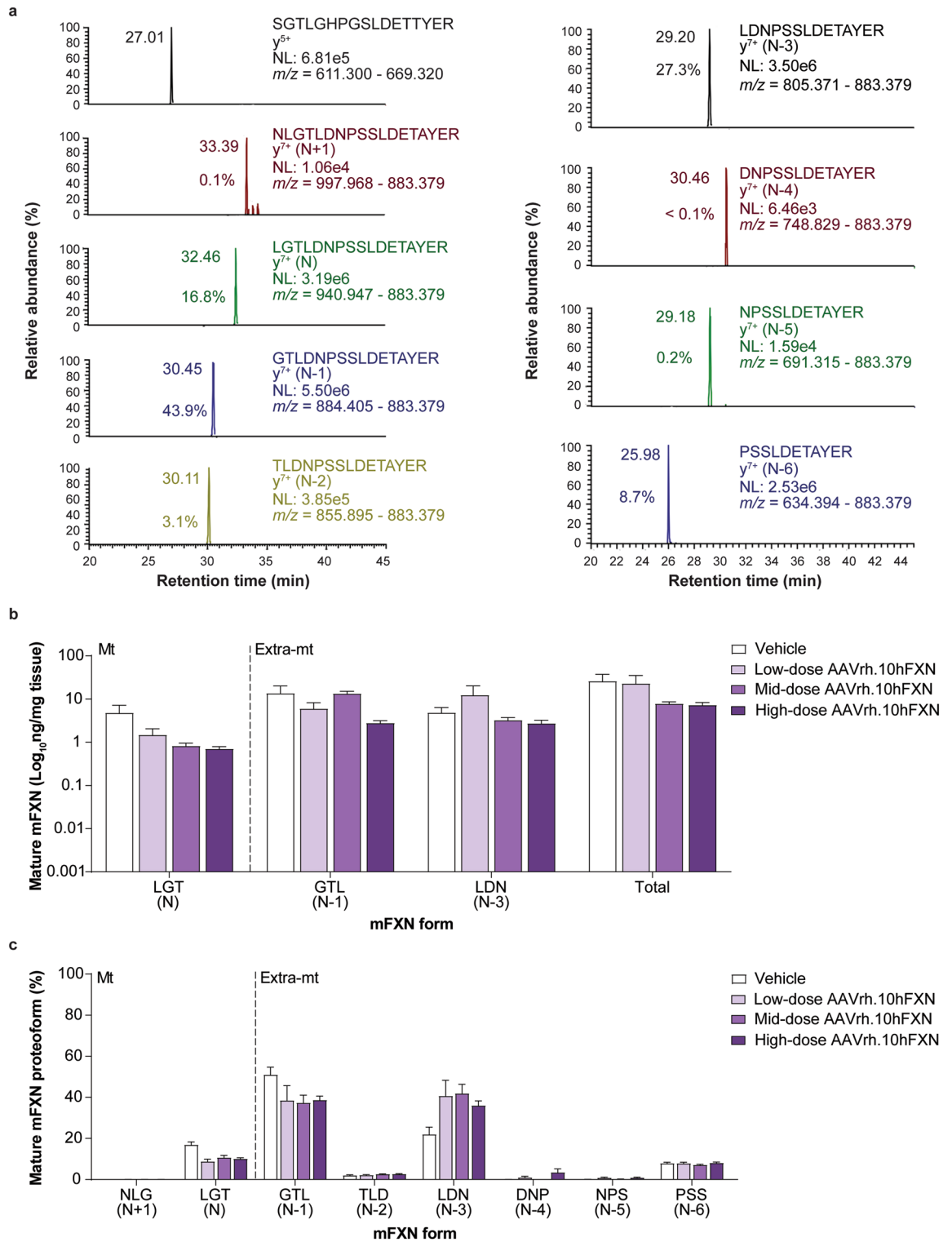
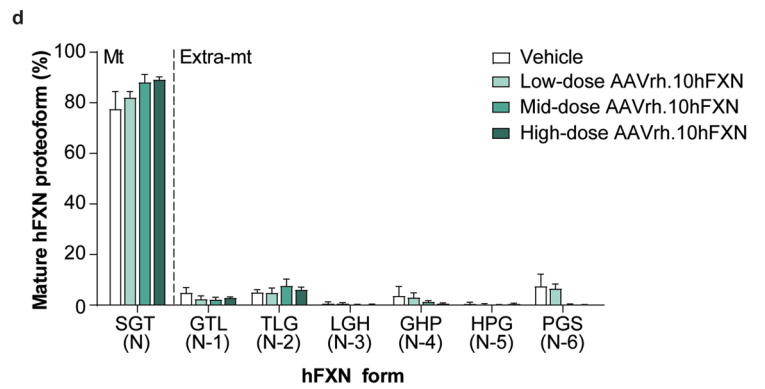
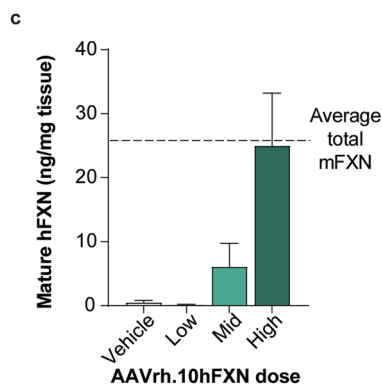
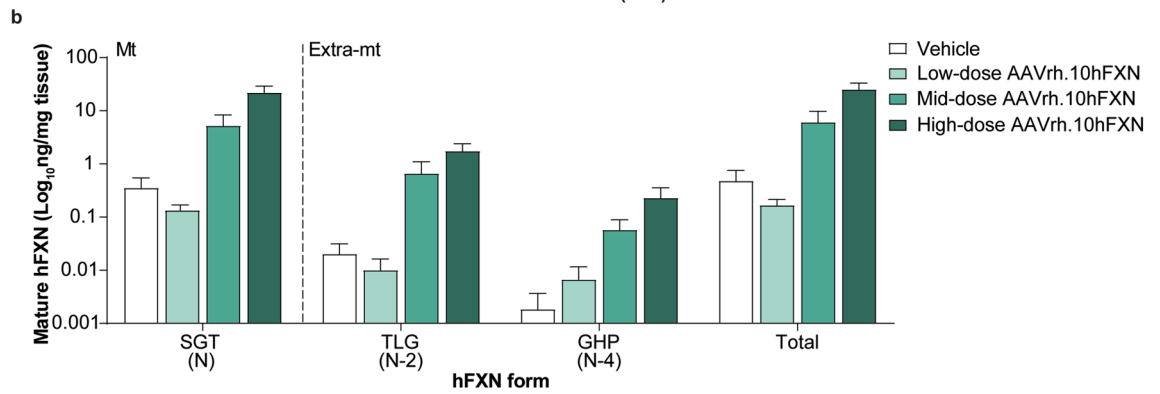
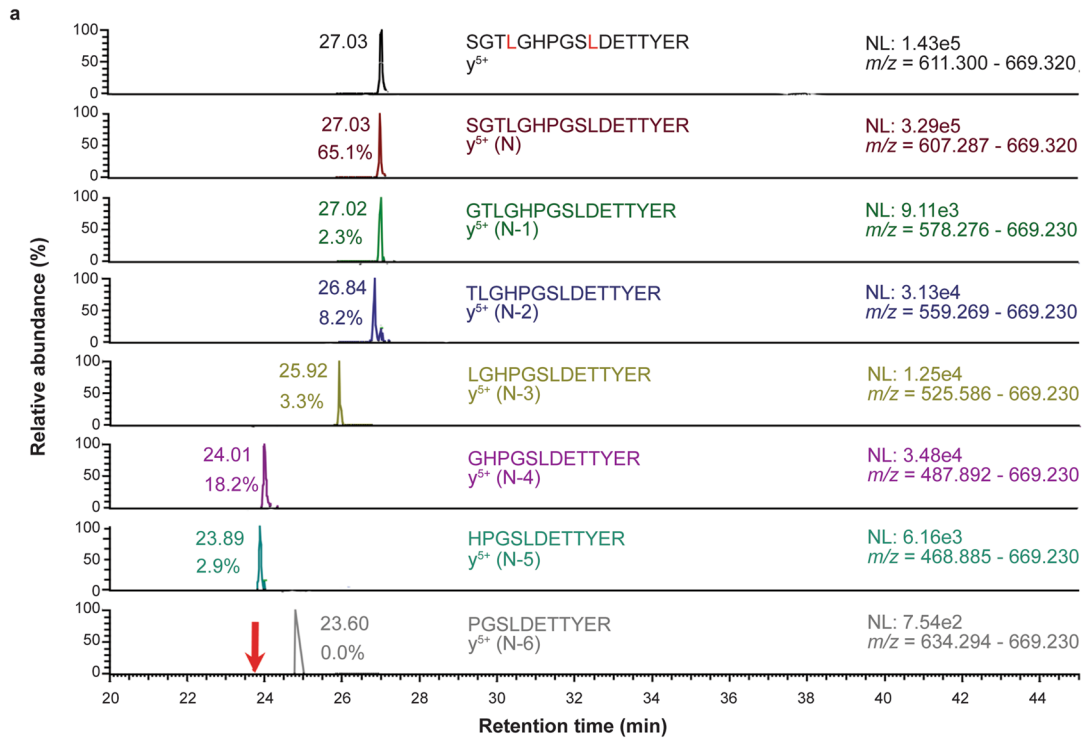


Figure 4. Detection and quantification of mature mFXN and its N-terminal tryptic peptides in the mouse liver following hFXN gene therapy. (a) Representative chromatograms from 2D-nano-UHPLC-PRM/HRMS analysis of mature mFXN N-terminal tryptic peptides in the liver of a mouse administered a high dose (1.8e13 gc/kg) of AAVrh.10hFXN. y-ion indicates the number of amino acids from the carboxy terminus that are present in this ion. Peptide retention times and relative amounts are shown on the left of the relevant signal. (b) Absolute concentrations of Mt and Extra-mt mature mFXN proteoforms in mouse liver after administration of one of three different doses of AAVrh.10hFXN (low-dose = 1.8e12 gc/kg, n = 6; mid-dose = 5.7e12 gc/kg, n = 6; high-dose = 1.8e13 gc/kg, n = 8) or vehicle (n = 5). (c) Relative amounts of mature mFXN in mice after administration of the same doses of AAVrh.10hFXN or vehicle (sample sizes as above). (b, c) Data are expressed as mean ± s.e.m. AAVrh.10hFXN = adeno-associated virus rhesus serotype 10 encoding human frataxin; 2D-nano-UHPLC-PRM/HRMS = two-dimensional nano-ultra-high performance liquid chromatography-parallel reaction monitoring high-resolution mass spectrometry; AAVrh.10hFXN = adeno-associated virus rhesus serotype 10 encoding human frataxin; Extra-mt = extra-mitochondrial; hFXN = human frataxin; mFXN = mouse frataxin; Mt = mitochondrial; m/z = mass-to-charge ratio; NL = normalized signal level; s.e.m. = standard error of the mean.



◀**Figure 5.** Detection and quantification of mature hFXN and its N-terminal tryptic peptides in the mouse heart following hFXN gene therapy. **(a)** Representative chromatograms from 2D-nano-UHPLC-PRM/HRMS analysis of mature hFXN N-terminal tryptic peptides in the heart of a mouse administered a high dose (1.8e13 gc/kg) of AAVrh.10hFXN. The red arrow indicates the retention time of the peptide. γ -ion indicates the number of amino acids from the carboxy terminus that are present in this ion. Peptide retention times and relative amounts are shown on the left of the relevant signal. **(b)** Absolute concentrations of Mt and Extra-mt mature hFXN proteoforms in mouse heart after administration of one of three different doses of AAVrh.10hFXN (low dose = 1.8e12 gc/kg, $n = 6$; mid dose = 5.7e12 gc/kg, $n = 4$; high dose = 1.8e13 gc/kg, $n = 8$) or vehicle ($n = 5$). While there were six mice treated with mid-dose AAVrh.10hFXN, insufficient heart sample precluded analysis of two mice. **(c)** Dose-dependent increase in total mature hFXN levels in mouse heart after administration of the same doses of AAVrh.10hFXN or vehicle (sample sizes as above). While there were six mice treated with mid-dose AAVrh.10hFXN, insufficient heart sample precluded analysis of two mice. The dotted line represents endogenous total mature mFXN levels (25.6 ng/mg). **(d)** Relative amounts of mature hFXN proteoforms in mouse heart after administration of the same doses of AAVrh.10hFXN or vehicle (sample sizes as above). **(b–d)** Data are expressed as mean \pm s.e.m. 2D-nano-UHPLC-PRM/HRMS = two-dimensional nano-ultra-high performance liquid chromatography-parallel reaction monitoring high-resolution mass spectrometry; AAVrh.10hFXN = adeno-associated virus rhesus serotype 10 encoding human frataxin; Extra-mt = extra-mitochondrial; hFXN = human frataxin; mFXN = mouse frataxin; Mt = mitochondrial; m/z = mass-to-charge ratio; NL = normalized signal level; s.e.m. = standard error of the mean.

Table S4). The relative abundance of the N form (compared with truncated mFXN forms) in mouse liver was 11.3% (Fig. 4c and Supplementary Table S4), and similar to mouse heart findings, approximated N-proteoform levels found in mice not subjected to gene therapy in a previous study³¹. The extra-mitochondrial N-1 form was the most abundant mFXN proteoform and represented 40.8% of total mature mFXN (Fig. 4c). Consistent with previous studies³¹, a substantial amount of the N-3 truncated form (35.8%) was detected in the mouse liver. The N + 1 peptide (monitored to determine the presence of elongated forms of mFXN) represented an overall mean of only 0.1% of total mFXN in the mouse liver ($n = 25$), indicating near-complete processing of full length/elongated mFXN into mature/truncated mFXN proteoforms (Fig. 4a and Supplementary Table S4).

Mature hFXN expression in mouse heart tissue following hFXN gene therapy

2D-nano-UHPLC-PRM/HRMS was used to detect mature hFXN following hFXN gene therapy and assess whether it underwent truncation similar to mFXN in the mouse heart. A representative chromatogram of mature hFXN in mouse heart tissue is shown in Fig. 5a. There was a robust detection of both N-terminal peptides representing mature SILAC-hFXN internal standard and mature hFXN. In addition, N-terminal truncations of hFXN were detected, which corresponded to the N-1, N-2, N-3, and N-6 extra-mitochondrial forms (Fig. 5a).

Mature hFXN was detected in all heart samples from mice treated with AAVrh.10hFXN (Fig. 5b and Supplementary Table S5). Levels of hFXN increased in a dose-dependent manner, with mean total mature hFXN in mouse heart tissue following administration of low-, mid-, or high-dose AAVrh.10hFXN (0.2, 6.1, and 25.0 ng/mg, respectively; Fig. 5c). At the highest dose, the mean total mature hFXN level was similar to the mean level of endogenous total mature mFXN (Fig. 5c). The mitochondrial N peptide represented 84.6% of total mature hFXN levels in the mouse heart (Fig. 5d and Supplementary Table S5). Of the 15.4% of mature hFXN that underwent truncation, a mean of 3.1% corresponded to the N-1 form and a mean of 5.8% corresponded to the N-2 form (Fig. 5d and Supplementary Table S5).

Mature hFXN expression in mouse liver tissue following hFXN gene therapy

A representative 2D-nano-UHPLC-PRM/HRMS chromatogram of mature hFXN in mouse liver is shown in Fig. 6a. Similar to heart tissue findings, there was a robust detection of mature hFXN N peptide in the livers of mice treated with low-, mid-, or high-dose AAVrh.10hFXN (Fig. 6b and Supplementary Table S6). Total mature hFXN levels increased in a dose-dependent manner (Fig. 6c), with higher heart hFXN levels being associated with higher hFXN liver levels (Figs. 5c and 6c). Mean levels of total mature hFXN in mouse liver tissue following administration of low-, mid-, or high-dose AAVrh.10hFXN were 24.7, 29.6, and 31.2 ng/mg, respectively (Fig. 6c).

Mature hFXN expressed in mouse liver tissue was most frequently identified in N-2 (15.2%) and N-4 (26.4%) forms (Fig. 6d), which contrasts with the relatively lower abundance of N-2 form found in the heart (5.8%; Fig. 5d). The relative amount of the hFXN N form (compared with truncated hFXN forms) was lower in liver (47.0%) versus heart tissues (84.6%; Figs. 5d, 6d, and Supplementary Tables S5 and S6).

Discussion

Several studies have shown the potential for AAV-based gene therapy to rescue the cardiac manifestations of FRDA^{25,37,38}, but its success has thus far been limited by difficulties with achieving and maintaining hFXN levels that are sufficiently efficacious but low enough to avoid cardiac toxicity and subsequent decline of efficacy^{25,26}. Given these challenges, novel gene replacement approaches for FRDA need to first undergo comprehensive analysis in animal models to test and optimize efficacy and to minimize toxicity prior to evaluating the therapeutic potential in patients. The deficiency of FXN observed in FRDA results in both neurotoxicity^{10,23} and cardiotoxicity²³. Neurodegeneration affects the dorsal root ganglia³⁹, the spinal cord⁴⁰, the cerebellum²⁰, and the dentate nucleus⁴⁰, which causes the neurodegeneration and ataxia and results in FRDA patients being wheelchair bound on average at 15-years of age⁴¹. The cardiotoxicity is manifested primarily as hypertrophic cardiomyopathy⁶, which results in death from heart failure typically in the fourth decade⁴¹. Targeting the brain and the heart

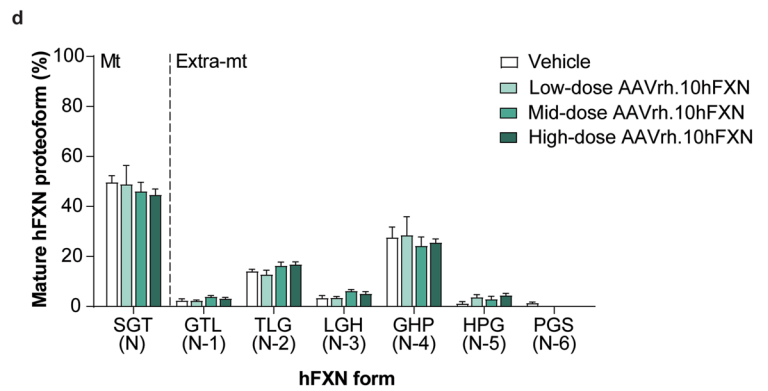
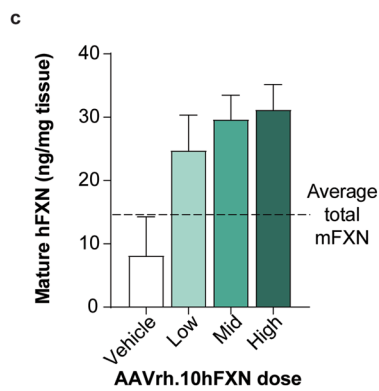
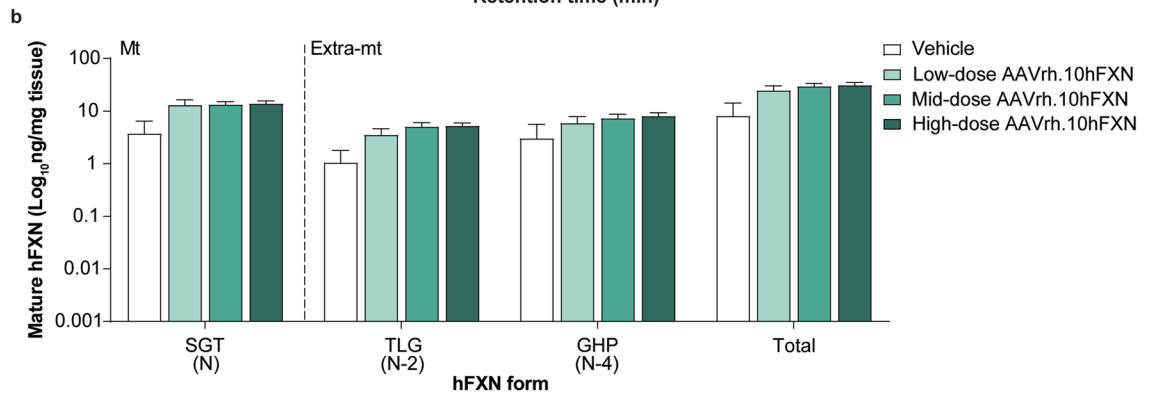
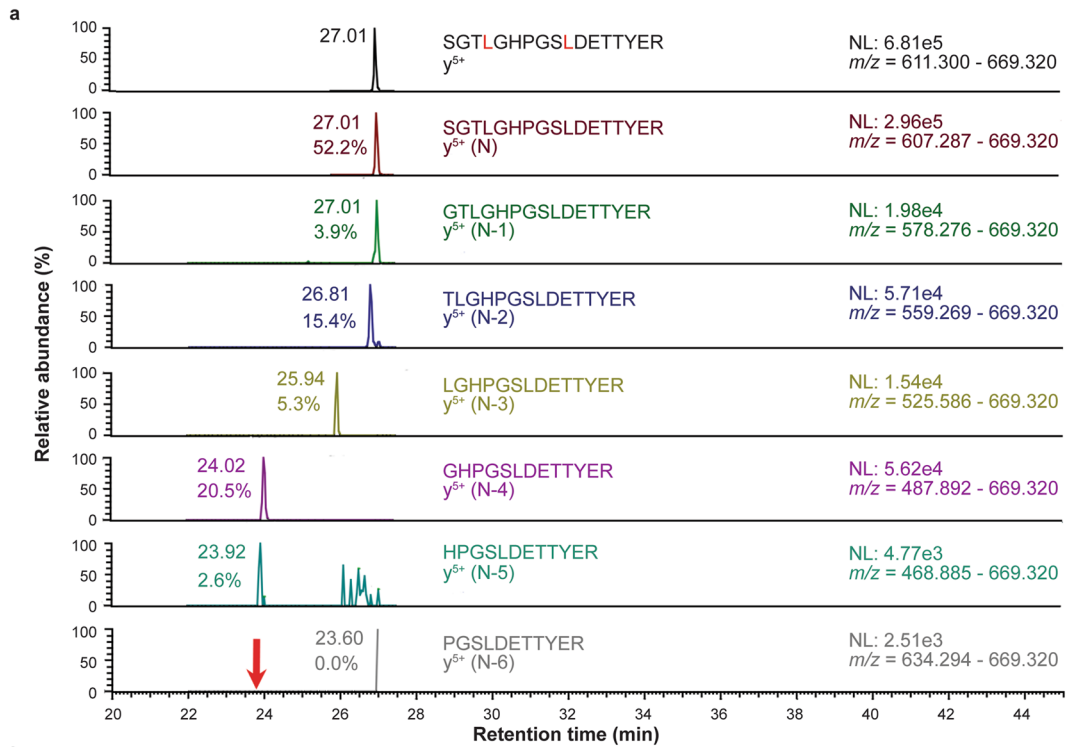


Figure 6. Detection and quantification of mature hFXN and its N-terminal tryptic peptides in the mouse liver following hFXN gene therapy. **(a)** Representative chromatograms from 2D-nano-UHPLC-PRM/HRMS analysis of mature hFXN N-terminal tryptic peptides in the liver of a mouse administered a high dose (1.8e13 gc/kg) of AAVrh.10hFXN. The red arrow indicates the retention time of the peptide. γ -ion indicates the number of amino acids from the carboxy terminus that are present in this ion. Peptide retention times and relative amounts are shown on the left of the relevant signal. **(b)** Absolute concentrations of Mt and Extra-mt mature hFXN in mouse liver after administration of one of three different doses of AAVrh.10hFXN (low-dose = 1.8e12 gc/kg, n = 6; mid-dose = 5.7e12 gc/kg, n = 6; high-dose = 1.8e13 gc/kg, n = 8) or vehicle (n = 5). **(c)** Dose-dependent increase in total mature hFXN levels in mouse liver after administration of the same doses of AAVrh.10hFXN or vehicle (sample sizes as above). The dotted line represents endogenous total mature mFXN levels (14.9 ng/mg). **(d)** Relative amounts of mature hFXN proteoforms in mouse liver after administration of the same doses of AAVrh.10hFXN or vehicle (sample sizes as above). **(b–d)** Data are expressed as mean \pm s.e.m. 2D-nano-UHPLC-PRM/HRMS = two-dimensional nano-ultra-high performance liquid chromatography-parallel reaction monitoring high-resolution mass spectrometry; AAVrh.10hFXN = adeno-associated virus rhesus serotype 10 encoding human frataxin; Extra-mt = extra-mitochondrial; hFXN = human frataxin; mFXN = mouse frataxin; Mt = mitochondrial; m/z = mass-to-charge ratio; NL = normalized signal level; s.e.m. = standard error of the mean.

together represents a formidable challenge and so our initial studies have focused on intravenous gene delivery and targeting to the heart.

Therefore, the aim of the present pre-clinical study was to evaluate hFXN expression following hFXN gene therapy in mice. The primary objective was to determine whether mature hFXN could be expressed at levels close to endogenous mature mFXN³¹ after administration of recombinant AAVrh.10 encoding hFXN (AAVrh.10hFXN). In addition, this study aimed to determine whether hFXN expressed in mouse tissues underwent truncation (similar to mFXN)³¹, a process that does not appear to occur to hFXN in human tissues³¹. We predicted that little toxicity would be observed with the low (1.8e12 gc/kg) or mid-dose of AAV vector (5.7e12 gc/kg) given to mice⁴². This contrast with reports that a higher dose of AAV vector can result in hFXN-M cardiac overexpression up to 20-fold higher than the normal endogenous mouse FXN-M levels and caused significant cardiotoxicity^{25,26}. Our prediction turned out to be correct as no cardiotoxicity were observed in the present study when mice were given similar doses to those that resulted in improved survival in an FRDA mouse model⁴². Furthermore, at these doses, the expressed hFXN protein levels (Fig. 5c) were comparable to the endogenous mouse mitochondrial FXN levels (Fig. 3c). Consequently, these pharmacokinetic data provided an important guide to initial doses of the AAV vector given to human subjects. However, we realize that prior to human studies, it might be good to confirm that gene therapy does not induce toxic side-effects in the mouse model by conducting assays to determine the oxygen consumption rate and the generation of reactive oxygen species as well as ensuring that there are no changes to mitochondrial biogenesis and dynamics.

The correlation between mRNA levels and protein expression is often weak in various tissues. Thus, in a xenograft model system, differentially expressed mRNAs demonstrated a significantly stronger correlation with expressed protein levels compared to non-differentially expressed mRNAs⁴³. Another study revealed that the correlation of mRNA to protein levels was poor to moderate (Pearson correlations ranged from 0 to 0.63), indicating that mRNA abundances poorly predict protein expression levels⁴⁴. Furthermore, protein levels are influenced by various conditions, including whether tissues are in a steady state, undergoing long-term state changes, or experiencing acute perturbation⁴⁵. As there is a documented poor relationship between differential mRNA and protein expression, we have chosen to focus on quantifying protein levels in the heart and liver as a more accurate predictor of hFXN over-expression resulting in the toxicity observed in other published studies^{25,26}.

Full-length mFXN is rapidly converted by MPP to mFXN in the mitochondria and so previous studies have been unable to detect the full-length FXN in the heart and liver of animal models^{31,34}. However, we considered the possibility that the MPP might be overwhelmed by the expression of full-length hFXN during gene therapy. Therefore, we analyzed the tryptic peptide N⁷⁷LGTLDNPSSLDEYER⁹⁷ that would arise from trypsin cleavage of full-length mouse FXN (Fig. 1). Only trace amounts of this tryptic peptide (0.1% of total FXN) was detected in mouse heart (Fig. 3a) or mouse liver (Fig. 4a) after gene therapy showing that almost undetectable amounts of elongated or full-length forms were present in either of these tissues. We recently reported a gene therapy study in non-human primates³⁴. This study revealed that there was a nonlinear response of hFXN expression in monkey hearts with increasing doses of the AAV vector but were unable to detect any truncated from of the hFXN or monkey FXN.

Findings from the present study demonstrate that IV administration of AAVrh.10hFXN gene therapy leads to dose-dependent cardiac and hepatic expression of mature hFXN in mice (Figs. 5d and 6d), and that hFXN undergoes processing (similar to endogenous mFXN) to produce truncated mature forms of hFXN that have not been observed in human tissues³¹. Unlike mFXN, which is primarily truncated to an N-1 form, AAVrh.10hFXN-delivered hFXN is primarily truncated to an N-2 form in mouse hearts (Fig. 3b). Though the impact of this differential processing of hFXN versus mFXN is unclear, AAVrh.10hFXN-derived total hFXN protein does not appear to be expressed at levels exceeding the average total endogenous mFXN level in mouse heart tissue (Fig. 5c), as has been previously reported in animal models^{25,26}.

Cytosolic full-length hFXN rapidly translocate to the mitochondria where it undergoes two sequential cleavages by MPP to produce mitochondrial mature hFXN containing the N-terminal tryptic peptide (S⁸¹GTLGHPGSLDETYER⁹⁷). Mature hFXN has never been detected outside of the mitochondria in humans⁴⁶. Therefore, it is reasonable to surmise that when full-length hFXN is expressed in the cytosol of mouse cells, it will similarly translocate to the mitochondria and undergo sequential MPP-mediated cleavages on the N-terminal

side of leucine-42 and serine-81 to give rise to mature hFXN (Fig. 1)^{28,29}. This mature hFXN form was the major form (80–90%) observed in the mouse heart following hFXN gene therapy (Fig. 3b). The lack of significant amounts of mature (N-1)-hFXN found in the mouse heart may be attributed to the amino-terminal sequence differences. Mature mFXN has an N-terminal leucine (Fig. 1), which violates the N-terminal end rule and is thus predicted to be metabolically unstable⁴⁷. In contrast, mature hFXN has a metabolically stable serine residue at its N-terminus (Fig. 1). At higher doses of AAVrh.10hFXN, mature (N-2)-hFXN accounted for approximately 6% of the total hFXN detected in the mouse heart, which was similar to the level of mature (N-1)-mFXN detected in the mouse heart (Supplementary Table S5). This suggests that the protease responsible for the cleavage of mature mFXN on the N-terminal side of glycine-79 might be responsible for cleavage of mature hFXN on the N-terminal side of threonine-83 (Fig. 1). Unlike the extra-mitochondrial location of the mature (N-1)-mFXN peptide, the sub-cellular localization of other truncated forms of mFXN in the mouse heart have not yet been delineated.

Compared with mouse heart, more abundant truncation of hFXN was observed in mouse liver, such that mature (N)-hFXN only accounted for 47.0% in the liver (Supplementary Table S6). Mature (N-2)- and (N-4)-hFXN were the other two major FXN proteoforms, accounting for 15.2% and 26.4% of the total mature hFXN, respectively. As was observed in mouse heart tissue, the enzyme responsible for generating mature (N-1)-mFXN in mouse liver generated very little mature (N-1)-hFXN (Supplementary Table S6). It is curious that mature (N-6)-hFXN was not detected in mouse liver (Supplementary Table S6), whereas larger amounts of cardiac and hepatic (N-6)-mFXN were detected (Supplementary Tables S3 and S4). It is conceivable that the protease responsible for generating mature (N-3)-mFXN in the liver (Supplementary Table S4) was also able to generate mature (N-4)-hFXN (Supplementary Table S6). However, the sub-cellular localization of these truncated forms of mFXN and hFXN in mouse liver remains unknown.

In contrast to the enzyme-linked immunosorbent assays (ELISAs) typically used for FXN detection, the 2D-nano-UHPLC-PRM/HRMS method can distinguish between mFXN and hFXN proteins within the same sample in a single assay. Unlike full-length mFXN, which is primarily processed to N and N-1 forms, full-length hFXN is primarily processed to N and N-2 forms in AAVrh.10hFXN-treated mouse hearts. The effect of this differential processing on treated mice is unclear, however the hFXN levels achieved in mouse heart were not highly overexpressed as has been previously reported to cause toxicity (Fig. 3c)²⁵. Furthermore, in other studies, administration of similar doses of AAVrh.10hFXN to mild or severe mouse models of FRDA improved the cardiac disease-relevant phenotypes without inducing the type of toxicity generally observed at the highest dose^{38,42}.

In summary, study results showed that IV administration of AAVrh.10hFXN at doses known to be effective in severe FRDA mouse models results in cardiac and hepatic mature hFXN levels that approximate endogenous mFXN levels in WT mice. The application of AAVrh.10hFXN gene therapy in patients with FRDA is currently being tested to examine the potential of delivering safe and therapeutic hFXN levels.

Data availability

All data generated or analyzed during this study are included in this published article and its Supplementary Information files. Any additional information can be obtained from the corresponding author upon reasonable request.

Received: 21 December 2023; Accepted: 6 April 2024

Published online: 10 April 2024

References

- Santos, R. *et al.* Friedreich ataxia: Molecular mechanisms, redox considerations, and therapeutic opportunities. *Antioxid Redox Signal.* **13**, 651–690. <https://doi.org/10.1089/ars.2009.3015> (2010).
- Kearney, M., Orrell, R. W., Fahey, M., Brassington, R. & Pandolfo, M. Pharmacological treatments for Friedreich ataxia. *Cochrane Database Syst. Rev.* <https://doi.org/10.1002/14651858.CD007791.pub4> (2016).
- Tsirikos, A. I. & Smith, G. Scoliosis in patients with Friedreich's ataxia. *J. Bone Joint Surg. Br.* **94**, 684–689. <https://doi.org/10.1302/0301-620X.94B5.28391> (2012).
- Rodden, L. N., Rummey, C., Dong, Y. N. & Lynch, D. R. Clinical evidence for variegated silencing in patients with Friedreich ataxia. *Neurol. Genet.* **8**, e683. <https://doi.org/10.1212/NXG.0000000000000683> (2022).
- Weidemann, F. *et al.* The cardiomyopathy in Friedreich's ataxia—new biomarker for staging cardiac involvement. *Int. J. Cardiol.* **194**, 50–57. <https://doi.org/10.1016/j.ijcard.2015.05.074> (2015).
- Norrish, G. *et al.* Friedreich's ataxia-associated childhood hypertrophic cardiomyopathy: A national cohort study. *Arch. Dis. Child.* **107**, 450–455. <https://doi.org/10.1136/archdischild-2021-322455> (2022).
- Tsou, A. Y. *et al.* Mortality in Friedreich ataxia. *J. Neurol. Sci.* **307**, 46–49. <https://doi.org/10.1016/j.jns.2011.05.023> (2011).
- Pousset, F. *et al.* A 22-year follow-up study of long-term cardiac outcome and predictors of survival in Friedreich Ataxia. *JAMA Neurol.* **72**, 1334–1341. <https://doi.org/10.1001/jamaneurol.2015.1855> (2015).
- Piguet, F. *et al.* Rapid and complete reversal of sensory ataxia by gene therapy in a novel model of Friedreich Ataxia. *Mol. Ther.* **26**, 1940–1952. <https://doi.org/10.1016/j.ymthe.2018.05.006> (2018).
- Ocana-Santero, G., Diaz-Nido, J. & Herranz-Martin, S. Future prospects of gene therapy for Friedreich's Ataxia. *Int. J. Mol. Sci.* <https://doi.org/10.3390/ijms22041815> (2021).
- Sivakumar, A. & Cherqui, S. Advantages and limitations of gene therapy and gene editing for Friedreich's ataxia. *Front. Genome Ed.* **4**, 903139. <https://doi.org/10.3389/fgeed.2022.903139> (2022).
- Bencze, K. Z. *et al.* The structure and function of frataxin. *Crit. Rev. Biochem. Mol. Biol.* **41**, 269–291. <https://doi.org/10.1080/10409230600846058> (2006).
- Pastore, A. & Puccio, H. Frataxin: A protein in search of a function. *J. Neurochem.* **126**(Suppl 1), 43–52. <https://doi.org/10.1111/jnc.12220> (2013).
- Campuzano, V. *et al.* Friedreich's ataxia: autosomal recessive disease caused by an intronic GAA triplet repeat expansion. *Science* **271**, 1423–1427 (1996).
- Campuzano, V. *et al.* Frataxin is reduced in Friedreich ataxia patients and is associated with mitochondrial membranes. *Hum. Mol. Genet.* **6**, 1771–1780 (1997).

16. Wang, Q. *et al.* Simultaneous quantification of mitochondrial mature frataxin and extra-mitochondrial Frataxin isoform E in Friedreich's Ataxia Blood. *Front. Neurosci.* **16**, 874768. <https://doi.org/10.3389/fnins.2022.874768> (2022).
17. Rojsajakul, T. *et al.* Liquid Chromatography-mass spectrometry analysis of frataxin proteoforms in whole blood as biomarkers of the genetic disease Friedreich's Ataxia. *Anal. Chem.* **95**, 4251–4260. <https://doi.org/10.1021/acs.analchem.3c00091> (2023).
18. Lill, R. *et al.* The role of mitochondria in cellular iron–sulfur protein biogenesis and iron metabolism. *Biochim. Biophys. Acta* **1823**, 1491–1508. <https://doi.org/10.1016/j.bbamcr.2012.05.009> (2012).
19. Weber, H. *et al.* Functional reconstitution of mitochondrial Fe/S cluster synthesis on Isu1 reveals the involvement of ferredoxin. *Nat. Commun.* **5**, 5013. <https://doi.org/10.1038/ncomms6013> (2014).
20. Bürk, K. Friedreich Ataxia: Current status and future prospects. *Cerebellum Ataxias* **4**, 4. <https://doi.org/10.1186/s40673-017-0062-x> (2017).
21. Chutake, Y. K., Lam, C., Costello, W. N., Anderson, M. & Bidichandani, S. I. Epigenetic promoter silencing in Friedreich ataxia is dependent on repeat length. *Ann. Neurol.* **76**, 522–528. <https://doi.org/10.1002/ana.24249> (2014).
22. Cook, A. & Giunti, P. Friedreich's ataxia: Clinical features, pathogenesis and management. *Br. Med. Bull.* **124**, 19–30. <https://doi.org/10.1093/bmb/ldx034> (2017).
23. Chiang, S., Kalinowski, D. S., Jansson, P. J., Richardson, D. R. & Huang, M.L.-H. Mitochondrial dysfunction in the neuro-degenerative and cardio-degenerative disease, Friedreich's ataxia. *Neurochem. Int.* **117**, 35–48 (2018).
24. Rodden, L. N. *et al.* DNA methylation in Friedreich ataxia silences expression of frataxin isoform E. *Sci. Rep.* **12**, 5031. <https://doi.org/10.1038/s41598-022-09002-5> (2022).
25. Belbellaa, B., Reutenauer, L., Messaddeq, N., Monassier, L. & Puccio, H. High levels of Frataxin overexpression lead to mitochondrial and cardiac toxicity in mouse models. *Mol. Ther. Methods Clin. Dev.* **19**, 120–138. <https://doi.org/10.1016/j.omtm.2020.08.018> (2020).
26. Huichalaf, C. *et al.* In vivo overexpression of frataxin causes toxicity mediated by iron-sulfur cluster deficiency. *Mol. Ther. Methods Clin. Dev.* **24**, 367–378. <https://doi.org/10.1016/j.omtm.2022.02.002> (2022).
27. Gakh, O., Cavadini, P. & Isaya, G. Mitochondrial processing peptidases. *Biochim. Biophys. Acta* **1592**, 63–77. [https://doi.org/10.1016/S0167-4889\(02\)00265-3](https://doi.org/10.1016/S0167-4889(02)00265-3) (2002).
28. Condo, I. *et al.* In vivo maturation of human frataxin. *Hum. Mol. Genet.* **16**, 1534–1540 (2007).
29. Schmucker, S., Argentini, M., Carelle-Calmels, N., Martelli, A. & Puccio, H. The in vivo mitochondrial two-step maturation of human frataxin. *Hum. Mol. Genet.* **17**, 3521–3531. <https://doi.org/10.1093/hmg/ddn244> (2008).
30. Guo, L. *et al.* Characterization of a new N-terminally acetylated extra-mitochondrial isoform of frataxin in human erythrocytes. *Sci. Rep.* **8**, 17043. <https://doi.org/10.1038/s41598-018-35346-y> (2018).
31. Weng, L. *et al.* Extra-mitochondrial mouse frataxin and its implications for mouse models of Friedreich's ataxia. *Sci. Rep.* **10**, 15788. <https://doi.org/10.1038/s41598-020-72884-w> (2020).
32. Guo, L. *et al.* Liquid chromatography-high resolution mass spectrometry analysis of platelet frataxin as a protein biomarker for the rare disease Friedreich's Ataxia. *Anal. Chem.* **90**, 2216–2223. <https://doi.org/10.1021/acs.analchem.7b04590> (2018).
33. du Percie Sert, N. *et al.* Reporting animal research: Explanation and elaboration for the ARRIVE guidelines 2.0. *PLoS Biol.* **18**, e3000411. <https://doi.org/10.1371/journal.pbio.3000411> (2020).
34. Rojsajakul, T. *et al.* Quantification of human mature frataxin protein expression in nonhuman primate hearts after gene therapy. *Commun. Biol.* **6**, 1093. <https://doi.org/10.1038/s42003-023-05472-z> (2023).
35. MacLean, B. *et al.* Skyline: An open source document editor for creating and analyzing targeted proteomics experiments. *Bioinformatics* **26**, 966–968. <https://doi.org/10.1093/bioinformatics/btq054> (2010).
36. Xia, H. *et al.* Novel frataxin isoforms may contribute to the pathological mechanism of Friedreich ataxia. *PLoS One* **7**, e47847. <https://doi.org/10.1371/journal.pone.0047847> (2012).
37. Perdomini, M. *et al.* Prevention and reversal of severe mitochondrial cardiomyopathy by gene therapy in a mouse model of Friedreich's ataxia. *Nat. Med.* **20**, 542–547. <https://doi.org/10.1038/nm.3510> (2014).
38. Salami, C. O. *et al.* Stress-induced mouse model of the cardiac manifestations of Friedreich's Ataxia corrected by AAV-mediated gene therapy. *Hum. Gene Ther.* **31**, 819–827. <https://doi.org/10.1089/hum.2019.363> (2020).
39. Monfort, B., Want, K., Gervason, S. & D'Autreaux, B. Recent advances in the elucidation of frataxin biochemical function open novel perspectives for the treatment of Friedreich's Ataxia. *Front. Neurosci.* **16**, 838335. <https://doi.org/10.3389/fnins.2022.838335> (2022).
40. Gonzalez-Cabo, P. & Palau, F. Mitochondrial pathophysiology in Friedreich's Ataxia. *J. Neurochem.* **126**(Suppl 1), 53–64. <https://doi.org/10.1111/jnc.12303> (2013).
41. Hanson, E., Sheldon, M., Pacheco, B., Alkubeysi, M. & Raizada, V. Heart disease in Friedreich's ataxia. *World J. Cardiol.* **11**, 1–12. <https://doi.org/10.4330/wjcv11.i1.1> (2019).
42. Munoz-Zuluaga, C. *et al.* Identification of safe and effective intravenous dose of AAVrh10h.FXN to treat the cardiac manifestations of friedreich's ataxia. *Hum. Gene Ther.* **34**, 605–615. <https://doi.org/10.1089/hum.2023.020> (2023).
43. Koussounadis, A., Langdon, S. P., Um, I. H., Harrison, D. J. & Smith, V. A. Relationship between differentially expressed mRNA and mRNA-protein correlations in a xenograft model system. *Sci. Rep.* **5**, 10775. <https://doi.org/10.1038/srep10775> (2015).
44. Pascal, L. E. *et al.* Correlation of mRNA and protein levels: Cell type-specific gene expression of cluster designation antigens in the prostate. *BMC Genom.* **9**, 246. <https://doi.org/10.1186/1471-2164-9-246> (2008).
45. Liu, Y., Beyer, A. & Aebersold, R. On the dependency of cellular protein levels on mRNA abundance. *Cell* **165**, 535–550. <https://doi.org/10.1016/j.cell.2016.03.014> (2016).
46. Martelli, A. *et al.* Frataxin is essential for extramitochondrial Fe-S cluster proteins in mammalian tissues. *Hum. Mol. Genet.* **16**, 2651–2658. <https://doi.org/10.1093/hmg/ddm163> (2007).
47. Varshavsky, A. The N-end rule: Functions, mysteries, uses. *Proc. Natl. Acad. Sci. USA* **93**, 12142–12149. <https://doi.org/10.1073/pnas.93.22.12142> (1996).

Acknowledgements

The authors wish to thank Brahim Belbellaa for critically reviewing the manuscript and Anju Nair for providing operational support for this study. Editorial assistance was provided by Lauren Todd and Holly Szczepanski of Sixsense Strategy Group and funded by LEXEO Therapeutics, Inc.

Author contributions

Conceptualization, N.S., R.K., and I.A.B.; data curation, T.R. and C.M.; formal analysis, N.S., R.K., and I.A.B.; investigation, T.R., N.S., C.M., and R.K.; funding acquisition, I.A.B.; methodology, T.R., C.M. and I.A.B.; supervision and project administration, N.S., C.M., R.K., and I.A.B. writing—original draft preparation, N.S., C.M., R.K., and I.A.B.; writing—review, editing, and approval, T.R., N.S., B.D., J.B.R., S.M.K, D.S., R.G.C., C.M., P.J., R.K., and I.A.B.

Funding

The authors gratefully acknowledge the financial support of the Hamilton and Finneran families, Penn Medicine/CHOP FRDA Center of Excellence, and NIH grants U01NS114143 and P30ES013508. The in-life studies were supported, in part, by NIH grant R61HL151355 and by LEXEO Therapeutics, Inc.

Competing interests

N.S., P.J., and R.K. are full-time employees of LEXEO Therapeutics, Inc. S.M.K. and D.S. have equity in LEXEO Therapeutics, Inc. and R.G.C. has equity in and is a consultant for LEXEO Therapeutics, Inc. I.A.B. has paid service/sponsored research agreements with LEXEO Therapeutics, Inc and Design Therapeutics, Inc. The other authors declare no competing interests.

Additional information

Supplementary Information The online version contains supplementary material available at <https://doi.org/10.1038/s41598-024-59060-0>.

Correspondence and requests for materials should be addressed to I.A.B.

Reprints and permissions information is available at www.nature.com/reprints.

Publisher's note Springer Nature remains neutral with regard to jurisdictional claims in published maps and institutional affiliations.



Open Access This article is licensed under a Creative Commons Attribution 4.0 International License, which permits use, sharing, adaptation, distribution and reproduction in any medium or format, as long as you give appropriate credit to the original author(s) and the source, provide a link to the Creative Commons licence, and indicate if changes were made. The images or other third party material in this article are included in the article's Creative Commons licence, unless indicated otherwise in a credit line to the material. If material is not included in the article's Creative Commons licence and your intended use is not permitted by statutory regulation or exceeds the permitted use, you will need to obtain permission directly from the copyright holder. To view a copy of this licence, visit <http://creativecommons.org/licenses/by/4.0/>.

© The Author(s) 2024